10th International Conference
12-14 July 2010
Southampton
RASD 2010

THE NONLINEAR DYNAMICS OF ELECTROSTATICALLY-ACTUATED, SINGLE-WALLED CARBON NANOTUBE RESONATORS

William G. Conley[1,2], Lin Yu[2,3], Molly R. Nelis[1,2], Arvind Raman[1,2], Charles M. Krousgrill[1], Saeed Mohammadi[2,4], and Jeffrey F. Rhoads[1,2,5*]

[1]School of Mechanical Engineering
Purdue University
585 Purdue Mall, West Lafayette, Indiana USA 47907
E-mail: jfrhoads@purdue.edu

[2]Birck Nanotechnology Center
Purdue University
1205 W. State St., West Lafayette, Indiana USA 47907

[3]Department of Physics
Purdue University
525 Northwestern Ave., West Lafayette, Indiana USA 47907

[4]School of Electrical Engineering
Purdue University
465 Northwestern Ave., West Lafayette, Indiana USA 47907

[5]Ray W. Herrick Laboratories
Purdue University
140 S. Martin Jischke Dr., West Lafayette, Indiana USA 47907

Keywords: Carbon Nanotubes; Resonator; Parametric Excitation

ABSTRACT

This work examines the nonlinear dynamics of suspended, electrostatically-actuated, single-walled carbon nanotube resonators. Specifically, the effort considers the near-resonant response of these systems under combined parametric and direct excitation, and characterizes the relative importance of these distinct excitation mechanisms, as well as an applied DC bias voltage, in a prototypical device design. Given the highly-nonlinear nature of the systems of interest, approximative multiphysics modeling and numerical continuation methods (AUTO) are used to predict the salient features of the nanoresonators' nonlinear response. The results of this analysis are highlighted within.

1. INTRODUCTION

Over the past decade, nanoelectromechanical resonators have garnered appreciable attention from the physics and engineering communities, due in part to their distinct potential in signal

processing, sensing, and electrical metrology applications [1, 2]. The interest in these nanoscale devices stems not only from their broad applicability, but also the inherent advantages that these systems have over their classical electrical and mechanical counterparts, including higher natural frequencies, lower power consumption, and improved compatibility with standard integrated circuit (IC) fabrication techniques. To date, research investigations of nanoscale resonators have largely focused on devices composed of single-walled carbon nanotubes (CNTs), or alternatively metallic or silicon nanowires, which are integrated with complementary electronics. While experimental advancements in this area have been frequent and noteworthy (see, for example, [1, 3, 4]), research emphasizing the modeling, analysis, and predictive design of CNT-based resonators is still in a state of infancy. Of particular note is the fact that most, if not all, of the previously proposed models for CNT resonators have captured only the simplest dynamic behaviors, using linear approximations to characterize small-amplitude responses or simple Duffing-like models to describe non-Lorentzian frequency responses exhibiting hysteresis [5, 6]. While these approaches may suffice in the predictive design of some devices, prior efforts in both the structural dynamics (see, for example, [7, 8]) and MEMS/NEMS (see, for example, [4, 9]) communities suggest that electrostatically-actuated CNT resonators are highly-nonlinear devices when driven above the thermomechanical noise floor and are capable of exhibiting a wide range of complex dynamic behaviors. Accordingly, there is a distinct need to develop high-fidelity nonlinear models for these systems, which can not only account for behaviors that are more complex than those predicted by existing models, but also facilitate the predictive design of future devices.

The present effort seeks to develop a refined understanding of the nonlinear dynamics of electrostatically-actuated, single-walled carbon nanotube resonators through the development, subsequent reduction, and analysis of a consistent multiphysics system model. This work builds upon prior efforts in the structural dynamics community, which have examined the nonlinear, non-planar behavior of strings and axisymmetric beams, and appends a force model capable of accounting for displacement-dependent electrostatic interactions. Given the need for brevity in this forum and the fact that the nonlinear dynamics of electrostatically-actuated CNT resonators are extremely rich, particular emphasis is placed here on characterizing the impact of both parametric excitation and applied DC bias voltages on a representative device.

2. MODELING

A representative electrostatically-actuated, single-walled carbon nanotube resonator is depicted pictorially and schematically in Fig. 1. The complete system consists of a nanotube of diameter d, length L, and flexural rigidity EI, which is suspended above a gate electrode with an initial separation distance of h. Given the axisymmetric nature of the resonator, both planar and non-planar displacement variables are used to describe the system's motion. The horizontal deflection of the system is specified by v, and the vertical deflection, which is coplanar with the applied variable-gap electrostatic force is specified by w. As noted in [9], this system is governed by a set of coupled, non-dimensional equations of motion given by

$$\begin{aligned} W_{,\tau\tau}+\frac{1}{Q}W_{,\tau}+\frac{1}{\beta^4}W_{,XXXX} &= \frac{1}{2R^2\beta^4}W_{,XX}\int_0^1\left[W_{,X}^2+V_{,X}^2\right]dX+F(X,\tau), \\ V_{,\tau\tau}+\frac{1}{Q}V_{,\tau}+\frac{1}{\beta^4}V_{,XXXX} &= \frac{1}{2R^2\beta^4}V_{,XX}\int_0^1\left[W_{,X}^2+V_{,X}^2\right]dX, \end{aligned} \tag{1}$$

where $W = w/h$ and $V = v/h$ represent the normalized vertical and horizontal deflections of the resonator, $R = [I/(Ah^2)]^{1/2}$ specifies the system's dimensionless radius of gyration (I and A represent the cross-sectional moment of inertia and area of the CNT, respectively), and β is

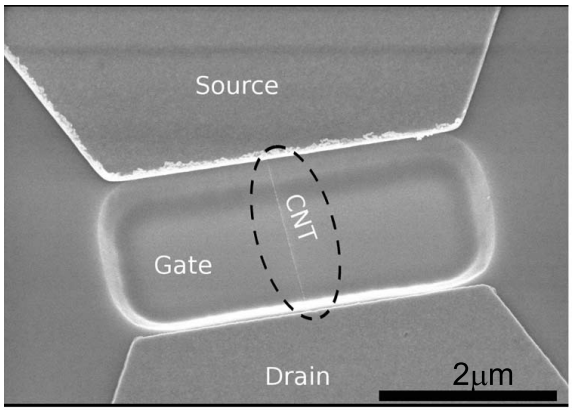

(a)

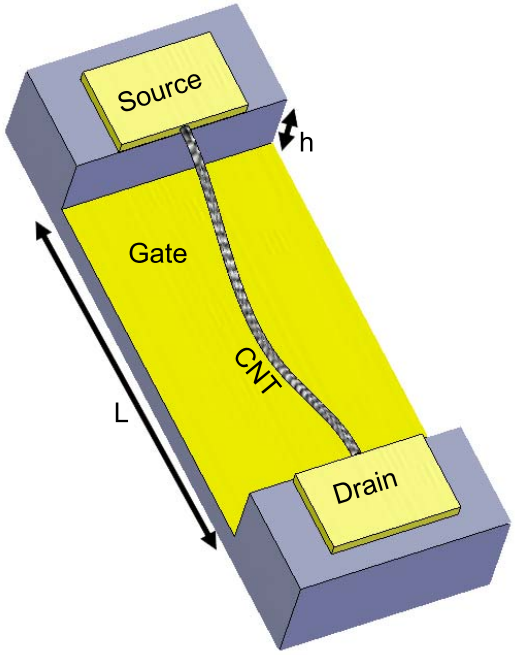

(b)

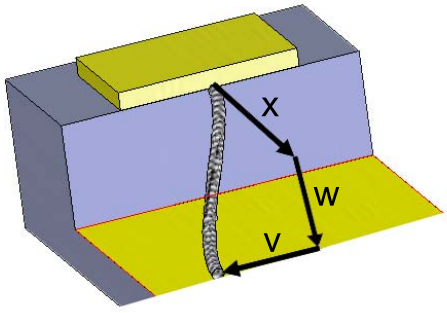

(c)

Figure 1: (a) Scanning electron micrograph of a representative, electrostatically-actuated single-walled carbon nanotube resonator suspended above a planar gate electrode. (b) A schematic representation of the electrostatically-actuated nanotube resonator. (c) Schematic highlighting the planar and non-planar displacement variables used to describe the motion of the CNT resonator. Note that the deflection w describes motions that are in the same plane as the applied force, while v captures the out-of-plane motions.

a numerical coefficient which depends on the mode of oscillation. Time is re-scaled here such that $\tau = \omega_0 t$, where ω_0 is the natural frequency of the system, and the dimensionless diameter and length are defined to be $D = d/h$ and $X = x/L$, respectively. Spatial partial derivatives are denoted by $(\cdot)_{,X}$, while temporal partial derivatives are specified by $(\cdot)_{,\tau}$. Dissipation, attributable to clamping losses and gas damping, is captured by an effective quality factor Q and the nondimensional force per unit length, which depends on the capacitance between the CNT and gate electrode, as well as the voltage difference $V_g(\tau)$, is denoted by $F(X,\tau)$ [4, 5, 9]. Assuming comparatively-small vibration amplitudes and minimal fringe field effects, the electrostatic force can be expanded in a Taylor series about $W = 0$ and represented as

$$\begin{aligned} F(X,\tau) =& \frac{S\pi\varepsilon_0 V_g^2(\tau)}{h^2}\frac{1}{(1-W)[\ln(4(1-W)/D)]^2} \\ \approx& \frac{S\pi\varepsilon_0 V_g^2(\tau)}{h^2}\left[f_0 + f_1 W + f_2 W^2 + f_3 W^3\right], \end{aligned} \tag{2}$$

where ε_0 is the permittivity of free space and $S = L^4/\beta^4 EI$ represents the compliance of the resonator. The coefficients f_n $(n = 0,1,2,3)$ are defined in Table 1. Note that this model assumes that there is no residual tension or slack in the CNT. In the presence of fabrication uncertainties, material imperfections, or chirality the system model will undoubtedly be more complex; however, these effects are largely beyond the scope of the present work.

To facilitate analysis, it proves convenient to perform a single-mode Galerkin projection on Eq. (1).[1] This results in a lumped-mass representation for the system given by

$$\begin{aligned} q_{1,\tau\tau} + \frac{1}{Q}q_{1,\tau} + q_1 + 8\alpha q_1[q_1^2 + q_2^2] =& V_g^2(\tau)[F_0 + F_1 q_1 + F_2 q_1^2 + F_3 q_1^3] \\ q_{2,\tau\tau} + \frac{1}{Q}q_{2,\tau} + q_2 + 8\alpha q_2[q_1^2 + q_2^2] =& 0. \end{aligned} \tag{3}$$

Here, the in-plane and out-of-plane displacement are denoted by $q_1(\tau)$ and $q_2(\tau)$, respectively, and the nonlinear stiffness coefficient is given by

$$\alpha = \frac{1}{16R^2\beta^4}\left[\int_0^1 \phi_{,X}^2\, dX\right]^2, \tag{4}$$

where $\phi(X)$ represents the particular eigenmode of interest. The electrostatic forcing coefficients F_n incorporated here are defined in Table 1. It is important to note that parametric excitation acts on both the linear and nonlinear parts of the model, as captured by F_1, F_2, and F_3, respectively. Time-varying excitation is provided by the periodic modulation of the gate voltage, $V_g(\tau)$.

While the resonator model detailed above captures a wide variety of planar, planar nonlinear, and non-planar nonlinear responses, it is important to note that it is founded upon a handful of limiting assumptions. For example, the use of a Taylor series approximation for the variable-gap electrostatic forces introduces some degree of error. Using the parameter values discussed in the subsequent section, one can show that the error in $F(X,\tau)$ is at most 10% for transverse deflections bounded by $W < 0.5$. Additionally, there is some error induced by the use of Galerkin projection. However, solving the static problem, $V_g = V_{dc}$ numerically through the use of the bvp5c routine in Matlab and comparing the result to the static deformation resulting from

[1] The Galerkin projection is identical to that presented in [9]: $W(X,\tau) = q_1(\tau)\phi(X)$ and $V(X,\tau) = q_2(\tau)\phi(X)$. Note that the eigenmode, $\phi(X)$, is assumed to be the fundamental mode of a linear clamped-clamped beam. For this mode, $\beta = 4.73$.

f_n in Eq. (2)	f_n	F_n in Eq. (3)	F_n ($1/V^2$)
$f_0 = \dfrac{1}{(\ln\chi)^2}$	0.0388	$F_0 = \dfrac{S\pi\varepsilon_0}{h^2} f_0 \displaystyle\int_0^1 \phi dX$	14.98
$f_1 = \dfrac{\ln\chi + 2}{(\ln\chi)^3}$	0.0541	$F_1 = \dfrac{S\pi\varepsilon_0}{h^2} f_1 \displaystyle\int_0^1 \phi^2 dX$	25.13
$f_2 = \dfrac{(\ln\chi)^2 + 3\ln\chi + 3}{(\ln\chi)^4}$	0.0663	$F_2 = \dfrac{S\pi\varepsilon_0}{h^2} f_2 \displaystyle\int_0^1 \phi^3 dX$	40.92
$f_3 = \dfrac{3(\ln\chi)^3 + 11(\ln\chi)^2 + 18\ln\chi + 12}{3(\ln\chi)^5}$	0.0771	$F_3 = \dfrac{S\pi\varepsilon_0}{h^2} f_3 \displaystyle\int_0^1 \phi^4 dX$	66.30

Table 1: Analytical and numerical expressions for the forcing parameters. Note that $\chi = 4/D$. The device geometry utilized here is detailed in Section 3.

the reduced-order model presented in Eq. (3) reveals that when $V_{dc} < 500$ mV there is at most a 1 nm error in the mid-span deflection (less than 1% of the initial gap height for the system considered herein). In light of these facts, the solutions of Eq. (3) should render a sufficiently accurate representation of the CNT's near-resonant response.

Previous works have adopted an applied excitation voltage of the form $V_g = V_{dc} + V_{ac}\sin(\Omega\tau)$ in their analyses of electrostatically-actuated nanoresonators (see, for example, [4]). This excitation results in a multiple frequency forcing proportional to $V_{dc}^2 + \frac{1}{2}V_{ac}^2 + 2V_{dc}V_{ac}\sin(\Omega\tau) - \frac{1}{2}V_{ac}^2\cos(2\Omega\tau)$. The complexity of this excitation model may be reduced when $V_{dc} \gg V_{ac}$, which leads to the harmonic excitation

$$V_g^2 \approx V_{dc}^2 + 2V_{dc}V_{ac}\sin(\Omega\tau). \tag{5}$$

In general, the aforementioned works have also assumed that the DC component of V_g^2 simply increases the linear natural frequency of the resonator and that one can approximate $V_g^2 \approx 2V_{dc}V_{ac}\sin(\Omega\tau)$. In contrast, this work considers the dynamic response of a representative CNT resonator excited by a voltage excitation signal of the form

$$V_g(\tau) = \sqrt{V_{dc}^2 + V_{ac}^2\sin(\Omega\tau)} \tag{6}$$

where $V_{dc}^2 > V_{ac}^2$ (this constraint is introduced to ensure physical consistency). This voltage signal, previously used in parametrically-excited MEMS devices [10], results in the harmonic excitation

$$V_g^2 = V_{dc}^2 + V_{ac}^2\sin(\Omega\tau) \tag{7}$$

and provides an exact form of the relationship in Eq. (5) without introducing *a priori* assumptions related to the effects of V_{dc}.

3. ANALYSIS

As highlighted in Eq. (3), the CNT resonators of interest are governed by a pair of coupled, nonlinear differential equations. While classical perturbation methods can be used to analyze this system in the weakly-nonlinear response regime, real device implementations are commonly driven with harder excitations. Accordingly, the present work adopts a numerical approach to analysis, which is founded upon the numerical continuation software AUTO [11].

To ensure consistency with ongoing experimental efforts, a 2.5 nm diameter, 1 μm long single-walled CNT is examined in this work. This device has a natural frequency of approximately 5.02 MHz, a quality factor of $Q = 25$, and a linear compliance of $S = 0.167$ m^2/N.

Note that these parameter values are representative of the devices fabricated in authors' group, (see Fig. 1) and match device 2 presented in [4], which was previously investigated in [9]. For present purposes, the CNT resonator is assumed to be suspended $h = 100$ nm above the gate electrode. This configuration results in a nonlinear stiffness coefficient $\alpha = 120.9$ and the values of f_n and F_n summarized in Table 1.

As noted in the introduction, the intent of this work is to highlight key features of the near-resonant response of electrostatically-actuated CNT resonators, and, more specifically, to characterize the impact of DC bias voltages and parametric excitations within these nonlinear systems. To facilitate this, three distinct excitation models are considered herein: (i) a model which ignores both DC bias voltage effects and parametric excitation – this model formed the basis of previous works [3, 4, 6, 9]; (ii) a model which includes a DC bias voltage, but neglects the effects of parametric excitation; and (iii) a model which includes both a DC bias voltage and parametric excitation. By systematically varying the applied voltage associated with each of these models, pertinent response characteristics can be attributed to the appropriate excitation mechanisms.

A series of benchmark frequency responses recovered when both the bias voltage and parametric excitation are neglected [i.e. when $V_g^2 \approx 2V_{dc}V_{ac}\sin(\Omega\tau)$] are depicted in Fig. 2. As noted above, adopting this form for the applied voltage results in the implicit assumption that the DC bias V_{dc}^2 does not affect the system's dynamic response. For small voltages, see Fig. 2(a), a near-linear response is recovered. As the excitation amplitude is increased, see Fig. 2(b), the system response becomes nonlinear and features substantial hysteresis (hardening) with respect to the drive frequency. Such responses have been observed experimentally in the work of Sazonova, et al. [4]. At large excitation voltages, see Fig. 2(c), a non-planar whirling branch is observed. This non-planar branch, previously discussed in [9], is of particular interest because no direct excitation mechanism excites the out-of-plane mode; rather, the trivial solution $q_2 = 0$ undergoes a fundamental transition as it becomes unstable, *even in the presence of dissipation.*

Using Fig. 2 as a benchmark, one can characterize the impact of DC bias voltages on the near-resonant response of suspended CNT resonators by examining the series of frequency responses depicted in Fig. 3, which are recovered by applying an equi-amplitude AC excitation in the absence of parametric excitations (i.e. with $F_1 = F_2 = F_3 = 0$). To ensure a harmonic excitation, a gate voltage of the form specified in Eq. (6) is applied in conjunction with a DC bias voltage of $V_{dc} = 100$ mV. Note that while the amplitude of this bias is approximately one order of magnitude smaller than those typically employed in experimentation [4], the qualitative findings of this paper are believed to have general validity.

A comparison of the frequency responses included in Figs. 2 and 3 reveals several features of note:

- As evident in Fig. 3, the bias voltage leads to a static deformation of the CNT away from resonance, which is not captured by the force model employed in Fig. 2.
- The near-resonance response is centered about $\Omega = 1$ in Fig. 2 and $\Omega \approx 2$ in Fig. 3. Physically, this increase in the resonator's natural frequency can be attributed to the mechanical tensioning caused by the applied DC bias voltage. Mathematically, this increase can be rectified by expanding q_1 according to $q_1 = q_{1dc} + q_{1ac}(\tau)$ and considering the resulting linear natural frequency, which is given by $\Omega = (1 + 24\alpha q_{1dc})^{1/2}$.
- In contrast to the Fig. 2, which predicts that the frequency response of the CNT resonator always hardens, Fig. 3 predicts that the resonator can exhibit mixed nonlinear behavior in the presence of a DC bias voltage, similar to that previously reported in [12], for example. Specifically, Figure 3(a) exhibits a slight softening behavior, while Fig. 3(b) shows a hysteretic softening response with a small region of hardening and Fig. 3(c) depicts a

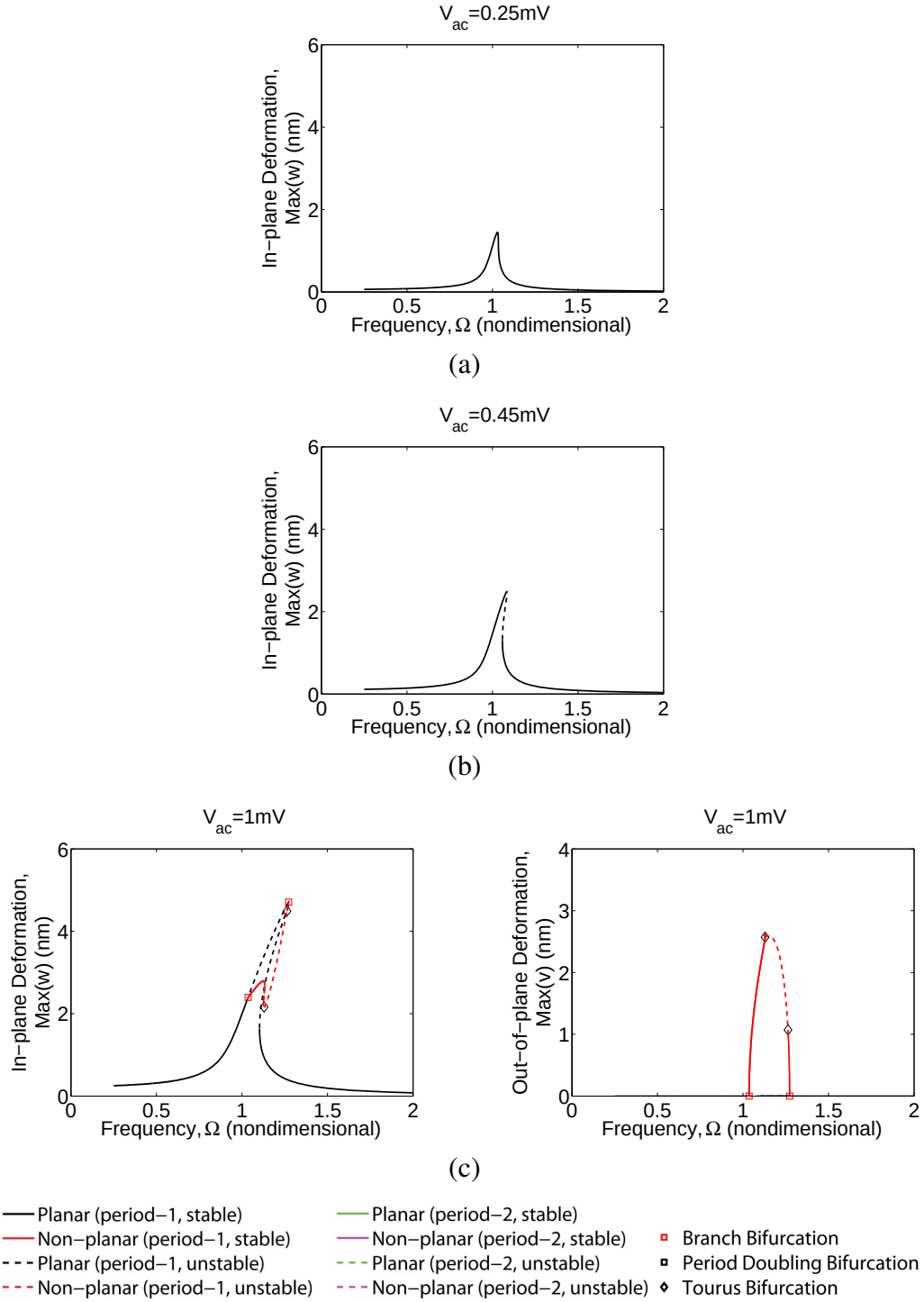

Figure 2: Simulation results recovered when the static deformation due to DC tension is neglected [i.e. $V_g^2 \approx 2V_{dc}V_{ac}\sin(\Omega\tau)$] and the parametric terms are neglected (i.e. $F_1 = F_2 = F_3 = 0$). In these figures $V_{dc} = 100$ mV. The peak deformation, at the center of the CNT, is presented as the excitation frequency is varied: (a) For small excitation voltages, such as $V_{ac} = 0.25$ mV, a linear response is predicted. (b) Intermediate excitation voltages, such as $V_{ac} = 0.45$ mV, result in hysteresis, which is attributable to mechanical hardening via the stretching nonlinearity. (c) Large excitation voltages, such as $V_{ac} = 1$ mV, result in non-planar, whirling motions. These motions can lose their stability via a torus bifurcation.

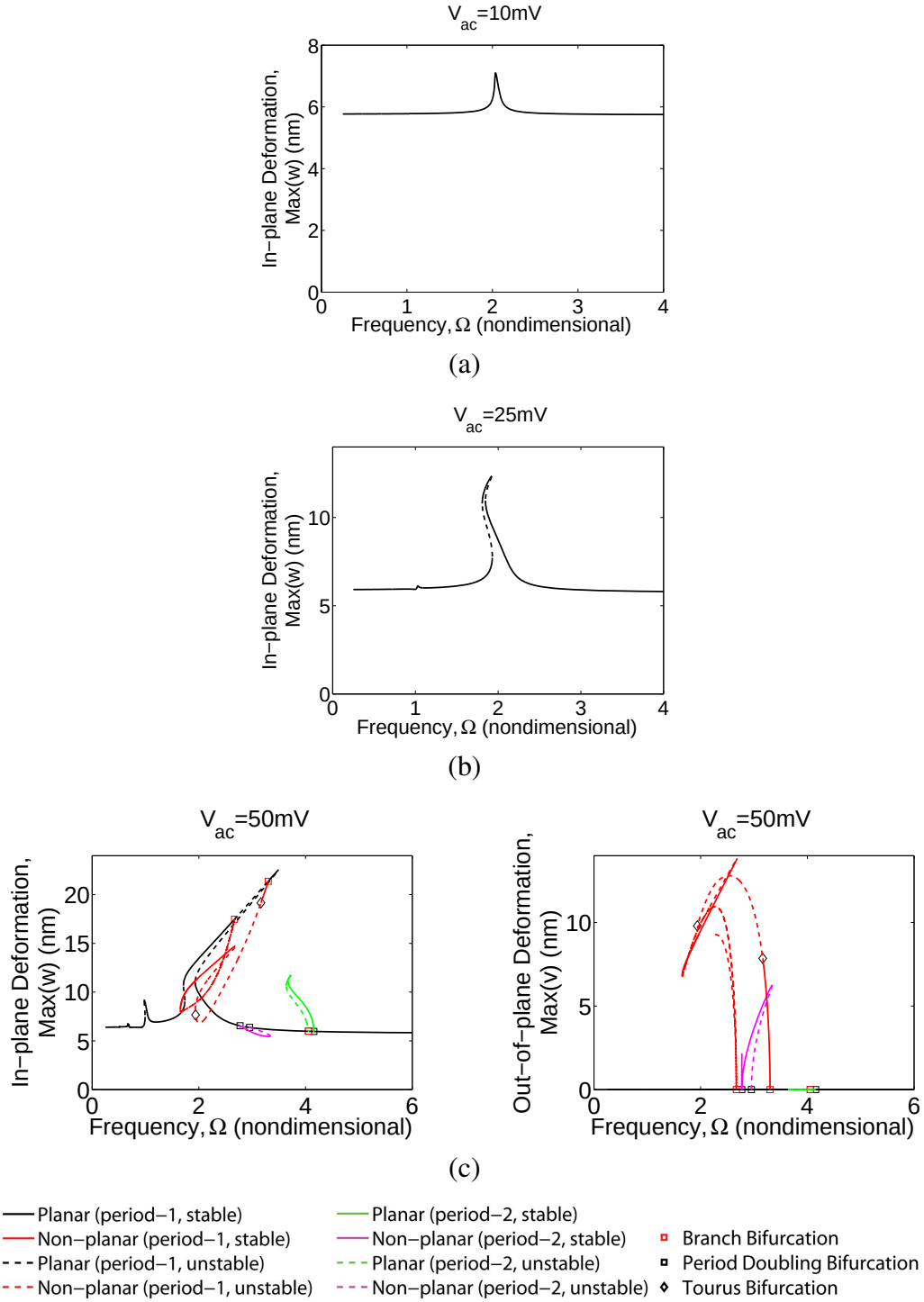

Figure 3: Simulation results recovered when all the parametric excitation terms are neglected (i.e. $F_1 = F_2 = F_3 = 0$), but a bias voltage of the form presented in Eq. (6) is included in the model. When a bias voltage of $V_{dc} = 100$ mV is applied, a deformation of 6 nm occurs and dynamic motions are superimposed on this deflection. (a) For small excitation voltages, $V_{ac} = 10$ mV, a linear response is observed. (b) Intermediate voltages, $V_{ac} = 25$ mV, produce a mixed softening-hardening response. (c) Large excitation voltages, $V_{ac} = 50$ mV, result in substantial hardening as well as non-planar branches. Additionally, period-2 solutions are observed; the green branch is a planar motion while the magenta solution has a large amplitude in the out-of-plane direction. Note that the additional bifurcations and solution branches presented here are attributable to the small deformation imparted by the bias voltage.

response which features a small region of softening and a large region of hardening. This complex backbone structure is a direct result of the asymmetric potential induced by the static deformation.

- The non-planar motions of the system increase in complexity with the inclusion of a DC bias. For example, in Fig. 2 the non-planar whirling motion, shown in red, simply hardens, while the non-planar branch, shown in Fig. 3, both softens and hardens.
- Additional planar and non-planar period-2 solutions are observed near $\Omega = 4$ and $\Omega = 3$, respectively, in the presence of a DC bias, see Fig. 3(c). Given the absence of parametric excitation present in the analyzed model, these solution branches are directly attributable to the quadratic nonlinearity, which results from the expansion $q_1 = q_{1_{dc}} + q_{1_{ac}}(\tau)$ briefly highlighted above.

To build upon the observations noted above, an additional large excitation voltage scenario ($V_{ac} = 85$ mV) is investigated, the results of which are shown in Fig. 4(a). As evident, the period-1 and period-2, planar and non-planar motions shown in Fig. 3(c) largely persist under larger excitation voltages. However, this persistence is accompanied by (i) an apparent destabilization of the planar primary resonant response, (ii) an enrichment of the system's superharmonic resonance structure, and (iii) a dramatic broadening of the period-1 and period-2, non-planar solutions' resonance bandwidth, all of which will have a dramatic impact on device operation.

To characterize the impact of linear and nonlinear parametric excitations on the near-resonant response of suspended CNTs, the system's behavior can be analyzed in both the absence and presence of the time-varying terms F_1, F_2, and F_3; see Fig. 4. For the device considered here parametric resonance is predicted to occur near $V_{ac} = 78$ mV in the presence of a $V_{dc} = 100$ mV bias, as validated by the instability boundary depicted in Fig. 5. Accordingly, the comparison is conducted at an excitation voltage in excess of the critical amplitude required to achieve parametric resonance. Two key results are of note:

- At excitation voltages in the proximity of the instability boundary, the amplitude of the CNT's planar response remains largely unchanged in the presence of resonant parametric excitations.
- There is an apparent parametric stabilization of the period-1, planar primary resonance branch in the presence of parametric excitations [13].

4. CONCLUSIONS

In conclusion, this work examined the nonlinear dynamics of a suspended, electrostatically-actuated single-walled carbon nanotube resonator. For the sake of brevity, particular emphasis was placed in this effort on characterizing the impact of DC bias voltages and parametric excitations on the system's near-resonant, nonlinear response. Ultimately, this work has demonstrated that (i) DC bias voltages have a greater impact on the nonlinear response of suspended CNT resonators than previously reported – these biases not only tune the linear natural frequency of the device, but also alter the qualitative nature of the system's nonlinear response; and (ii) parametric excitation likely affects the dynamic response of CNT resonators only at comparatively-large excitation voltages. Ongoing work is aimed at experimentally validating the results presented herein and developing a refined predictive design capability, which seeks to exploit pertinent nonlinear response features for practical gain where appropriate.

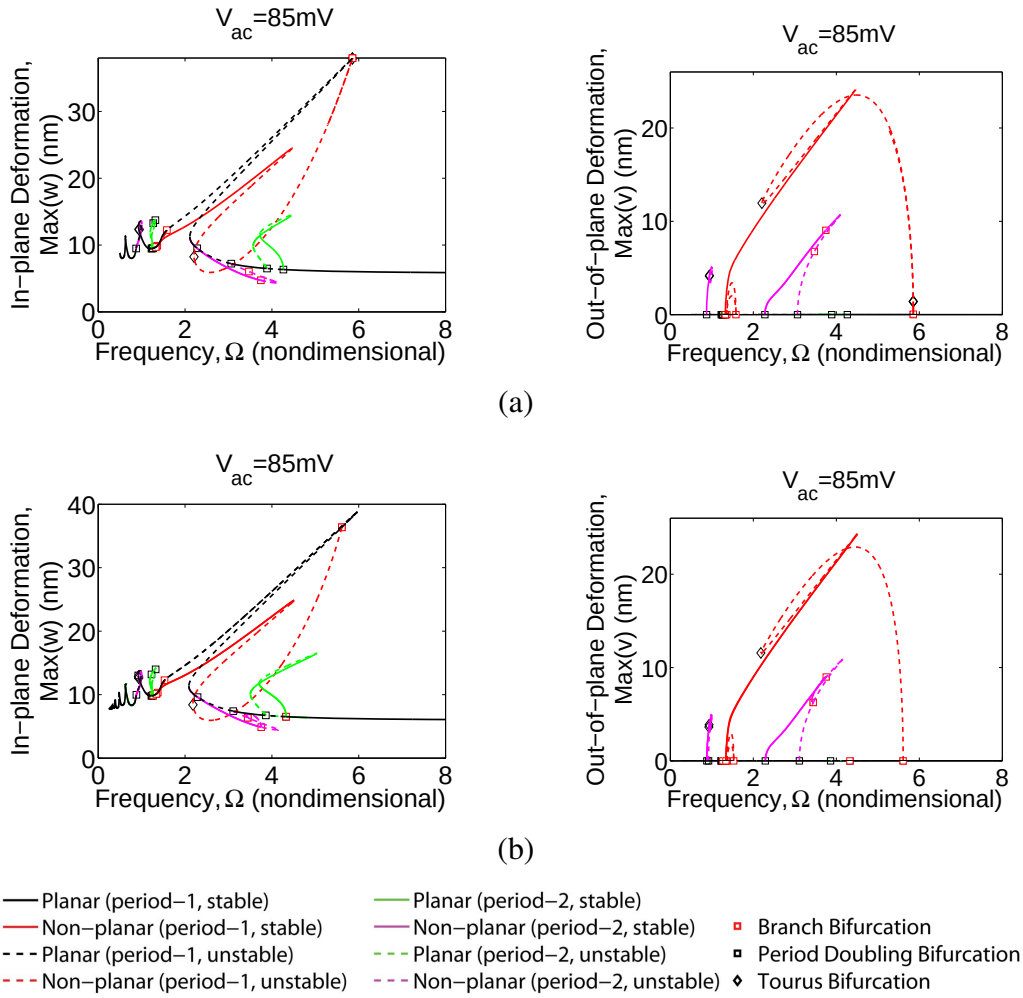

Figure 4: A frequency response comparison highlighting the relative importance of parametric excitation when a bias voltage of the form presented in Eq. (6) is included in the model. Note that a bias voltage of $V_{dc} = 100$ mV and excitation voltage of $V_{ac} = 85$ mV is considered. In sub-figure (a) parametric excitation is neglected (i.e. $F_1 = F_2 = F_3 = 0$), while in sub-figure (b) parametric excitation is included. Pertinent parameter values are included in Table 1. Note that for this excitation voltage, negligible differences are observed in the in-plane and out-of-plane responses.

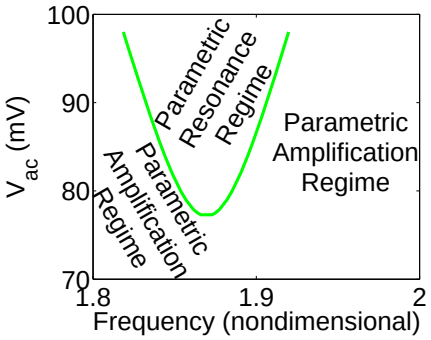

Figure 5: Regions of stability for the purely-parametric problem ($F_0 = F_2 = 0$). In the presence of dissipation, $Q = 25$, and bias, $V_{dc} = 100$ mV, parametric resonance only occurs if $V_{ac} > 78$ mV inside a limited frequency bandwidth centered near $\Omega = 1.9$. Parametric resonance refers to a large amplitude period-2 solution which bifurcates from the trivial solution.

ACKNOWLEDGMENTS

The effort detailed herein was supported by the Dynamical Systems Program of the National Science Foundation of the United States of America under grant 0826276. Any opinions, findings, conclusions, or recommendations expressed in this material are those of the authors and do not necessarily reflect those of the National Science Foundation.

REFERENCES

[1] H. B. Peng, C. W. Chang, S. Aloni, T. D. Yuzvinsky, A. Zettl, Ultrahigh frequency nanotube resonators. *Physical Review Letters*, 97, 087203, 2006.

[2] K. Jensen, K. Kim, A. Zettl, An atomic-resolution nanomechanical mass sensor. *Nature Nanotechnology*, 3, 533-537, 2008.

[3] B. Witkamp, M. Poot, H. S. J. van der Zant, Bending-mode vibration of a suspended nanotube resonator. *Nano Letters*, 6, 2904-2908, 2006.

[4] V. Sazonova, Y. Yaish, H. Ustunel, D. Roundy, T. A. Arias, P. McEuen, A tunable carbon nanotube electromechanical oscillator. *Nature*, 431, 284-287, 2004.

[5] M. Poot, B. Witkamp, M. A. Otte, H. S. J. van der Zant. Modelling suspended carbon nanotube resonators. *Physica Status Solidi (b)*, 244, 4252-4256, 2007.

[6] H. Ustunel, D. Roundy, and T. A. Arias, Modeling a suspended nanotube oscillator. *Nano Letters*, 5, 523-526, 2005.

[7] O. O'Reilly, P. J. Holmes, Non-linear, non-planar, and non-periodic vibrations of a string. *Journal of Sound and Vibration*, 153, 413-435, 1992.

[8] J. M. Johnson, A. K. Bajaj, Amplitude modulated and chaotic dynamics in resonant motion of strings. *Journal of Sound and Vibration*, 128, 87-107, 1989.

[9] W. G. Conley, A. Raman, C. M. Krousgrill, S. Mohammadi, Nonlinear and nonplanar dynamics of suspended nanotube and nanowire resonators. *Nano Letters*, 8, 1590-1595, 2008.

[10] K. L. Turner, S. A. Miller, P. G. Hartwell, N. C. MacDonald, S. H. Strogatz, S. G. Adams, Five parametric resonances in a microelectromechanical system. *Nature*, 396, 149-152, 1998.

[11] E. Doedel, A. Champneys, T. Fairgrieve, Y. Kuznetsov, B. Sandstede, X. Wang, AUTO 97: Continuation and Bifurcation Software for Ordinary Differential Equations, 1997.

[12] J. F. Rhoads, Exploring and exploiting resonance in coupled and/or nonlinear microelectromechanical oscillators. Ph.D. Dissertation, Michigan State University, 2007.

[13] S. Krylov, I. Harari, Y. Cohen, Stabilization of electrostatically actuated microstructures using parametric excitation. *Journal of Micromechanics and Mircoengineering*, 15, 1188-1204, 2005.